Supplementary Figures:

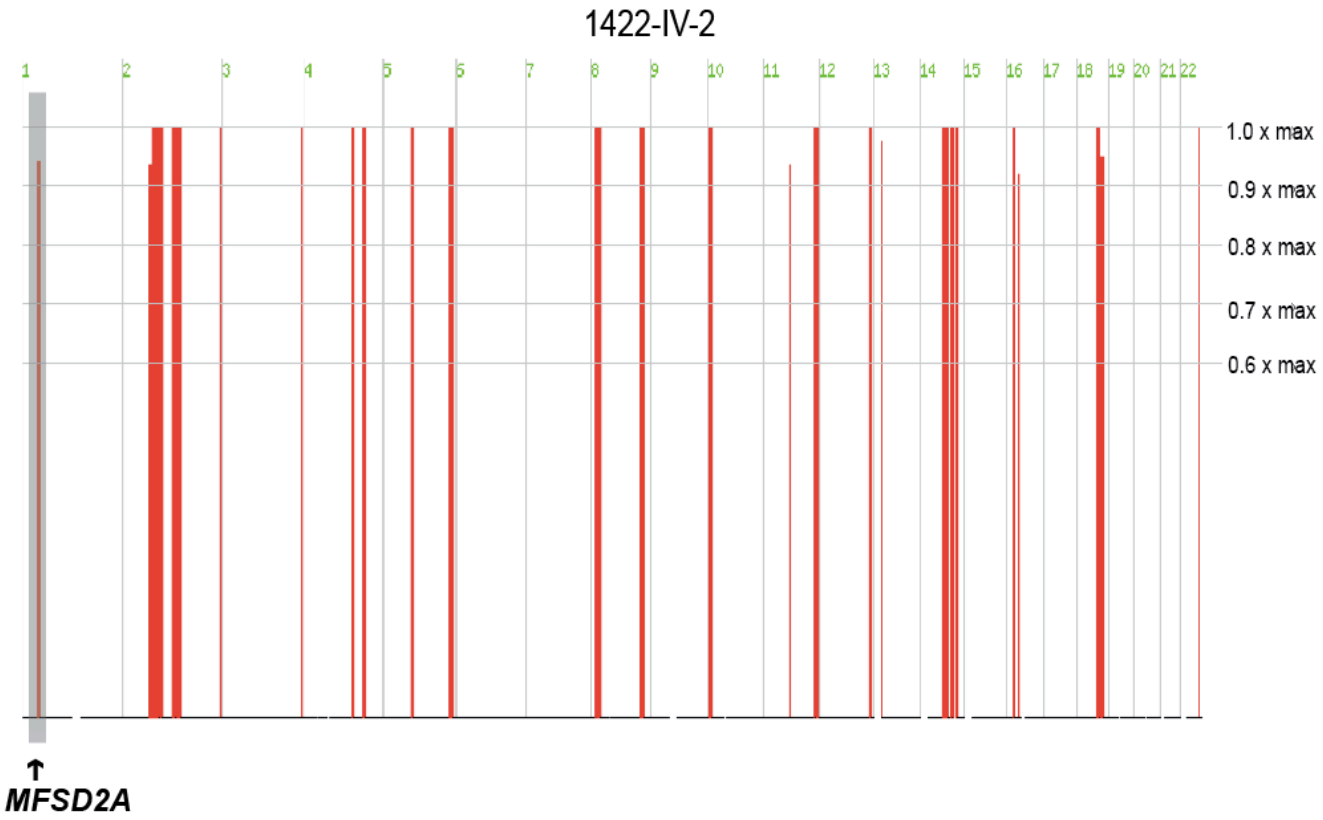

Supplementary Figure 1. Homozygosity map of affected individual from family 1422. Homozygosity plots showing homozygous blocks (red) in affected individuals from family 1422, with homozygous *MFSD2A* mutations. Gray: homozygous block comprising *MFSD2A* overlaps in all the affecteds. Arrow: location of *MFSD2A*.

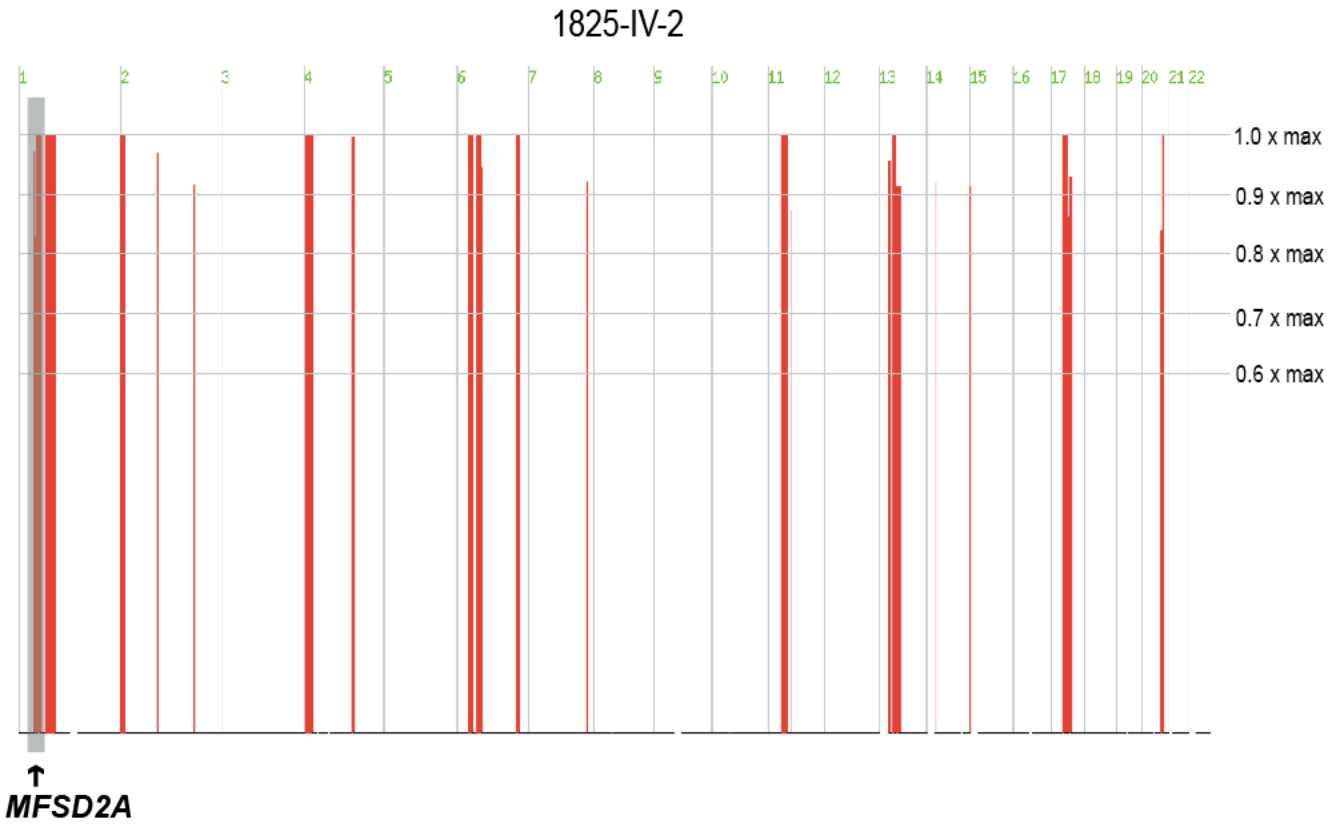

Supplementary Figure 2. Homozygosity map of affected individual from family 1825. Homozygosity plots showing homozygous blocks (red) in affected individuals from family 1825, with homozygous *MFSD2A* mutations. Gray: homozygous block comprising *MFSD2A* overlaps in all the affecteds. Arrow: location of *MFSD2A*.

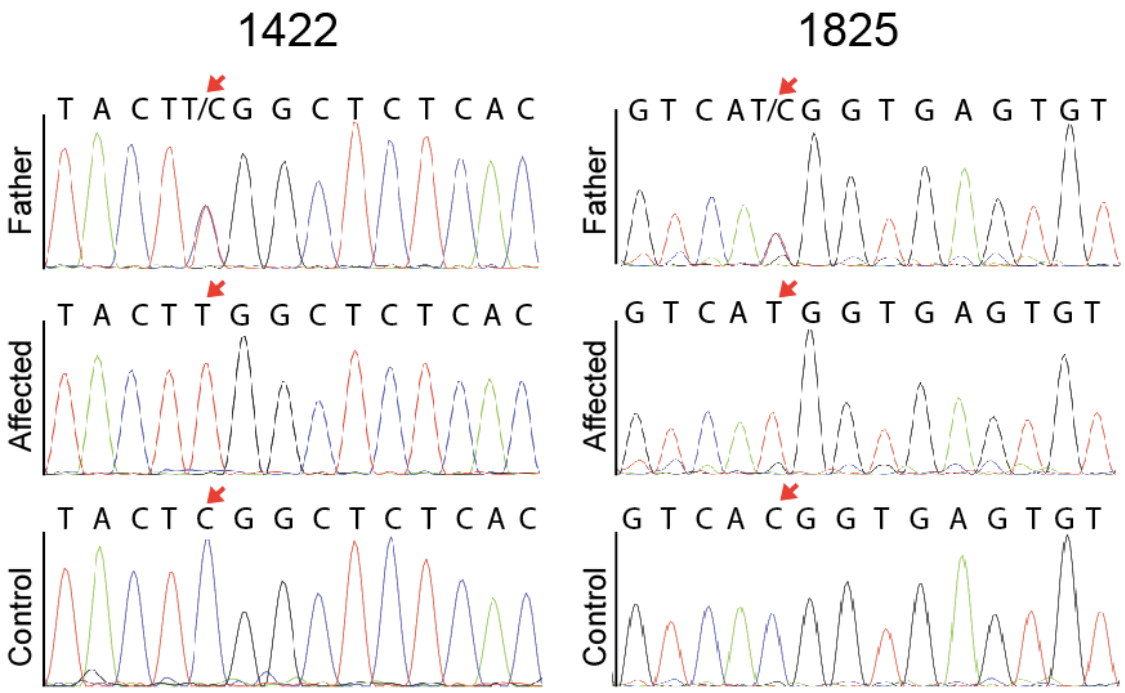

Supplementary Figure 3. Chromatograms from Sanger sequencing of father (heterozygous), affected (homozygous) and an unaffected sibling or non-related control (reference normal homozygous) showing the mutations (arrow).

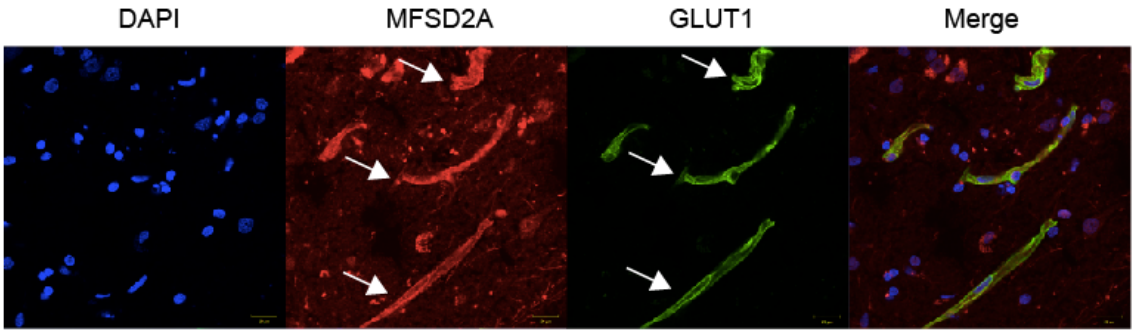

Supplementary Figure 4. MFSD2A is expressed in endothelial cells of microvessels in human fetal brain. MFSD2A (red) is highly expressed in endothelium and co-localizes with glucose transporter GLUT1 (green) in the human fetal brain. Arrows show endothelial cells in blood brain vessels. Scale bar 20μm.

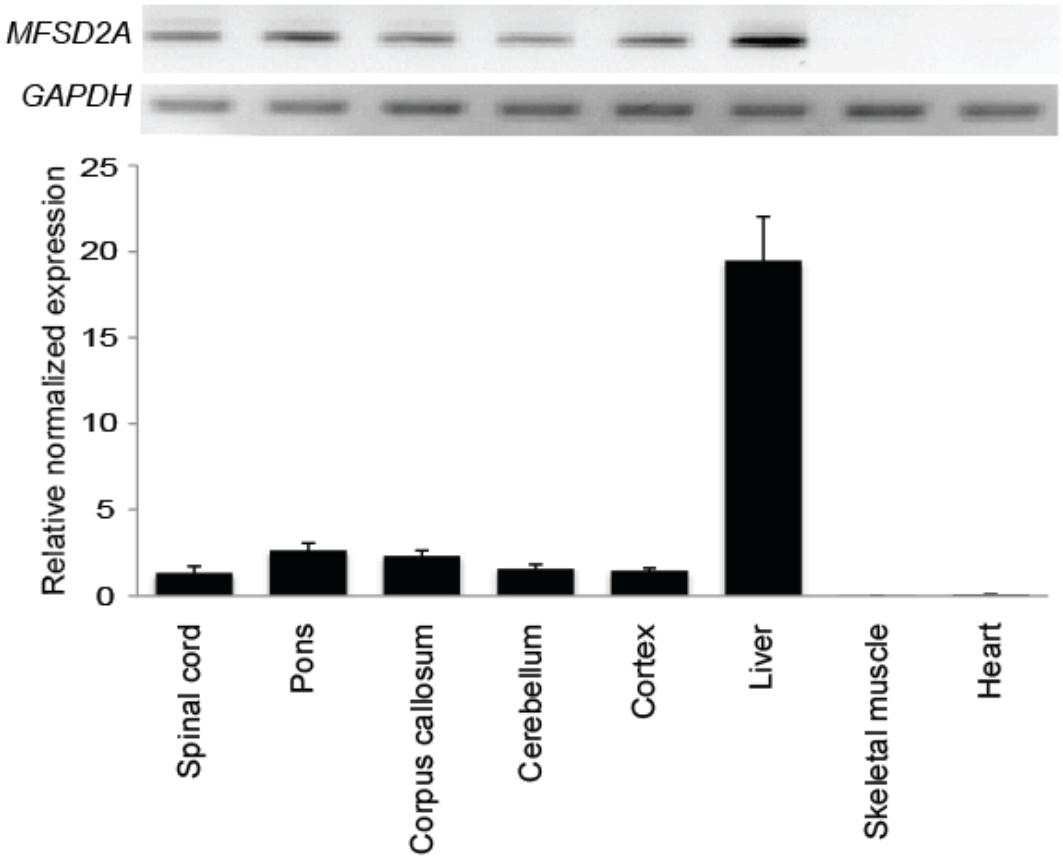

Supplementary Figure 5. Expression of *MFSD2A* in human tissues. RT-PCR (upper panel) and qPCR (lower panel) across human adult tissues shows expression in all tissues tested but skeletal muscle and heart. *GAPDH* was used as loading control.

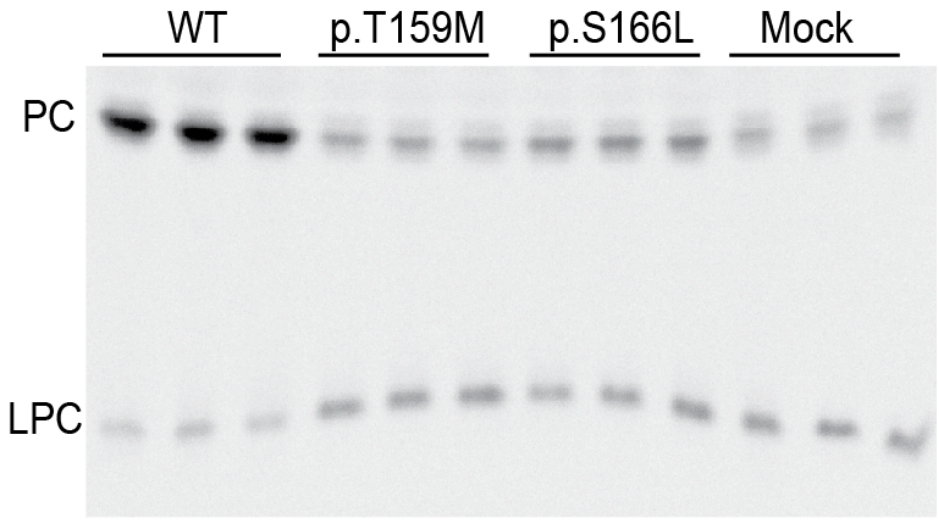

Supplementary Figure 6. Biological incorporation of radiolabeled LPC-[^{14}C]oleate into phosphatidylcholine (PC). Cells expressing human Mfsd2a (WT) and mutations p.T159M and p.S166L or empty plasmid were incubated with LPC-[^{14}C]oleate for 1hr. Lipids were extracted and analyzed using TLC for phospholipids. PC: phosphatidylcholine, LPC: lysophosphatidylcholine.

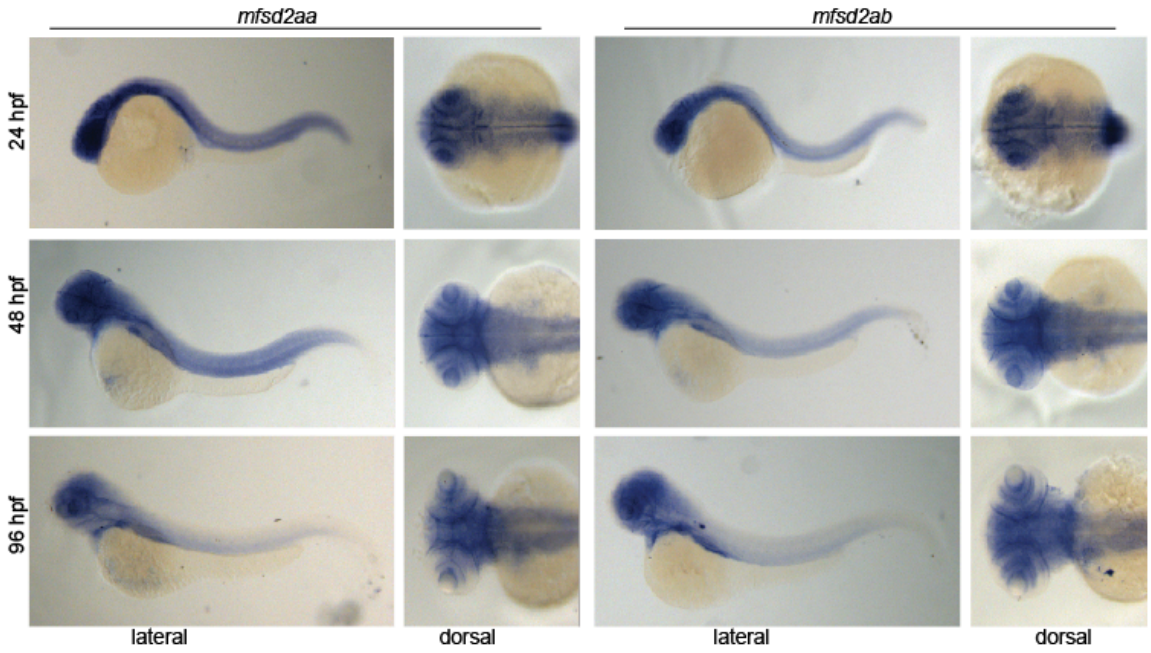

Supplementary Figure 7. *mfsd2aa* and *mfsd2ab* are expressed in the nervous system of zebrafish embryos. Whole mount embryo *in situ* hybridization of *mfsd2aa* and *mfsd2ab* riboprobes at 24, 48 and 96 hpf (hours post-fertilization). Both *mfsd2aa* and *mfsd2ab* were detected in the nervous system of zebrafish embryos at all stages examined.

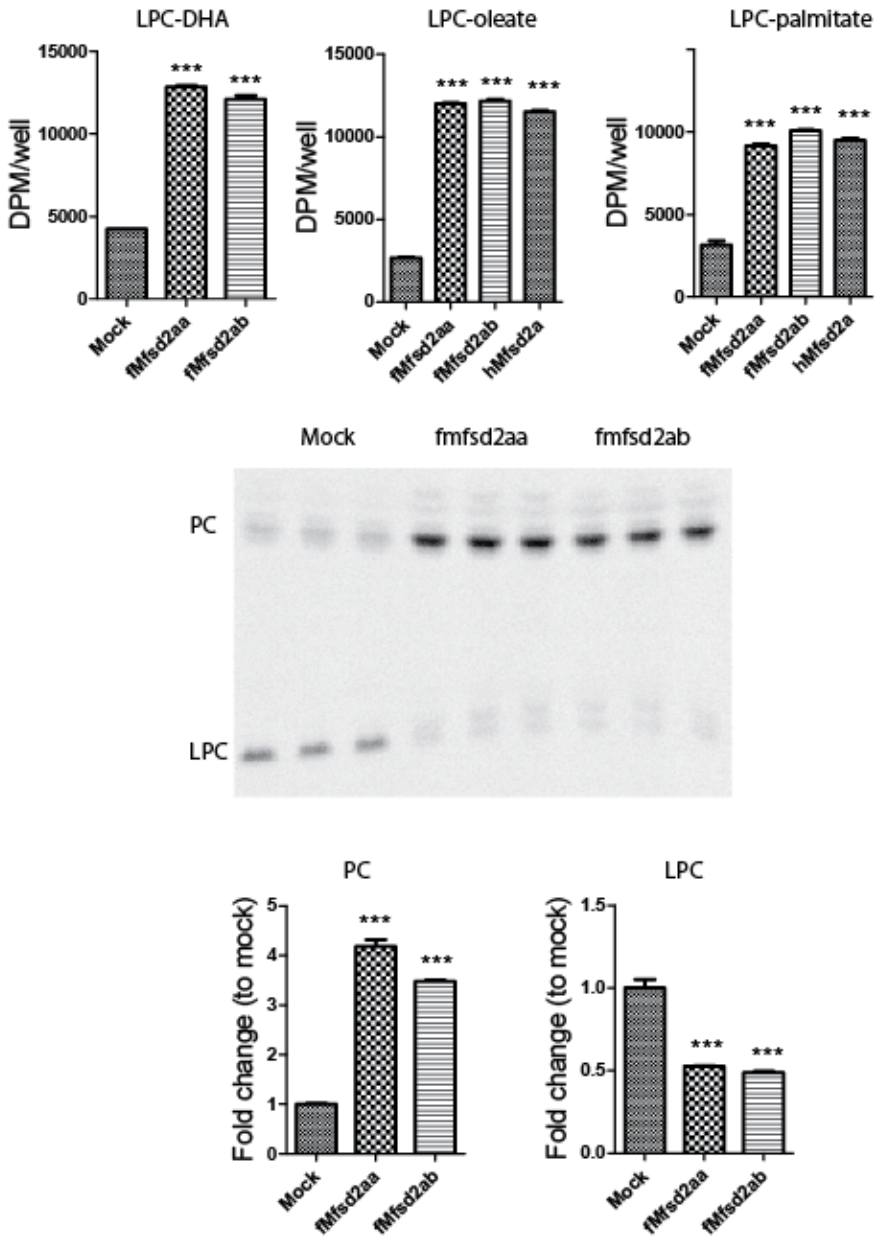

Supplementary Figure 8. Transport activity of zebrafish mfsd2aa and mfsd2ab. (a) Transport of 100μM LPC-[^{14}C]DHA, LPC-[^{14}C]oleate, or LPC [^{3}H]palmitate after 30 min of cells overexpressing with zebrafish mfsd2aa (fmfsd2aa) and mfsd2ab (fmfsd2ab) and human Mfsd2a proteins in HEK293 cells. **(b)** Biological incorporation of radiolabeled LPC-[^{14}C]oleate into phosphatidylcholine (PC). Cells expressing with fmfsd2aa and fmfsd2ab or empty plasmid were incubated with 100μM LPC-[^{14}C]oleate for 1hr. Lipids were extracted and analyzed using TLC for phospholipids. **(c)** quantification of PC and LPC bands from TLC plate shown in (b). PC: phosphatidylcholine, LPC: lysophosphatidylcholine. Experiments were performed twice with triplicates. Data are expressed as mean ± SEM. ***p<0.001.

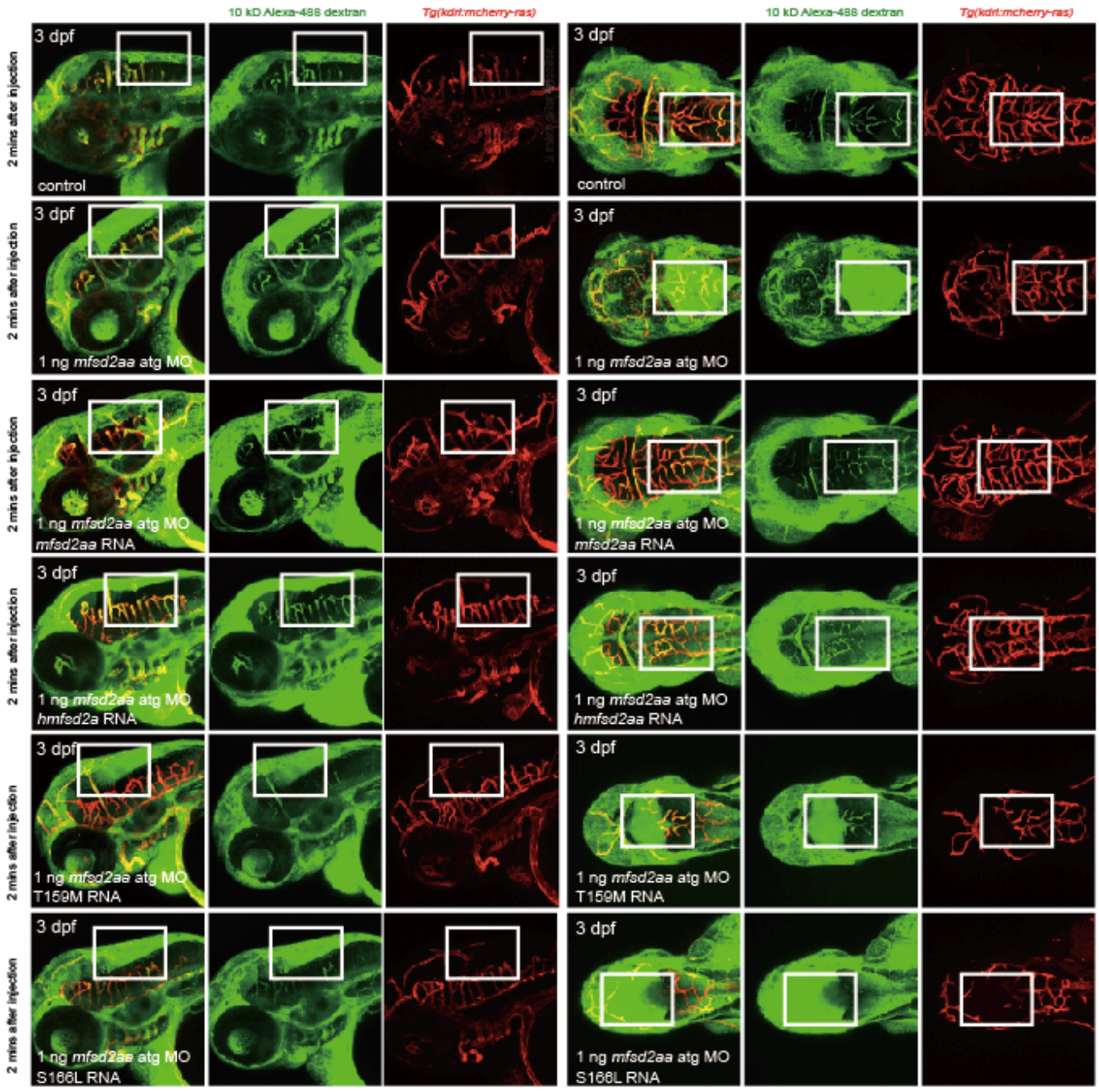

Supplementary Figure 9. 10 kD dextran injection. Intracardiac injection of 10-kD dextran into *mfsd2aa* morpholino (MO)-injected and control embryos. *mfsd2aa* MO (1ng) was co-injected with zebrafish wild-type *mfsd2aa* mRNA (50ng), human wild-type *MFSD2A* mRNA (50ng), or mutated p.T159M and p.S166L human *MFSD2A* mRNA (50ng). Colocalization of dextran (green) and cranial blood vessels (red). See **Supplementary videos 1-6**.

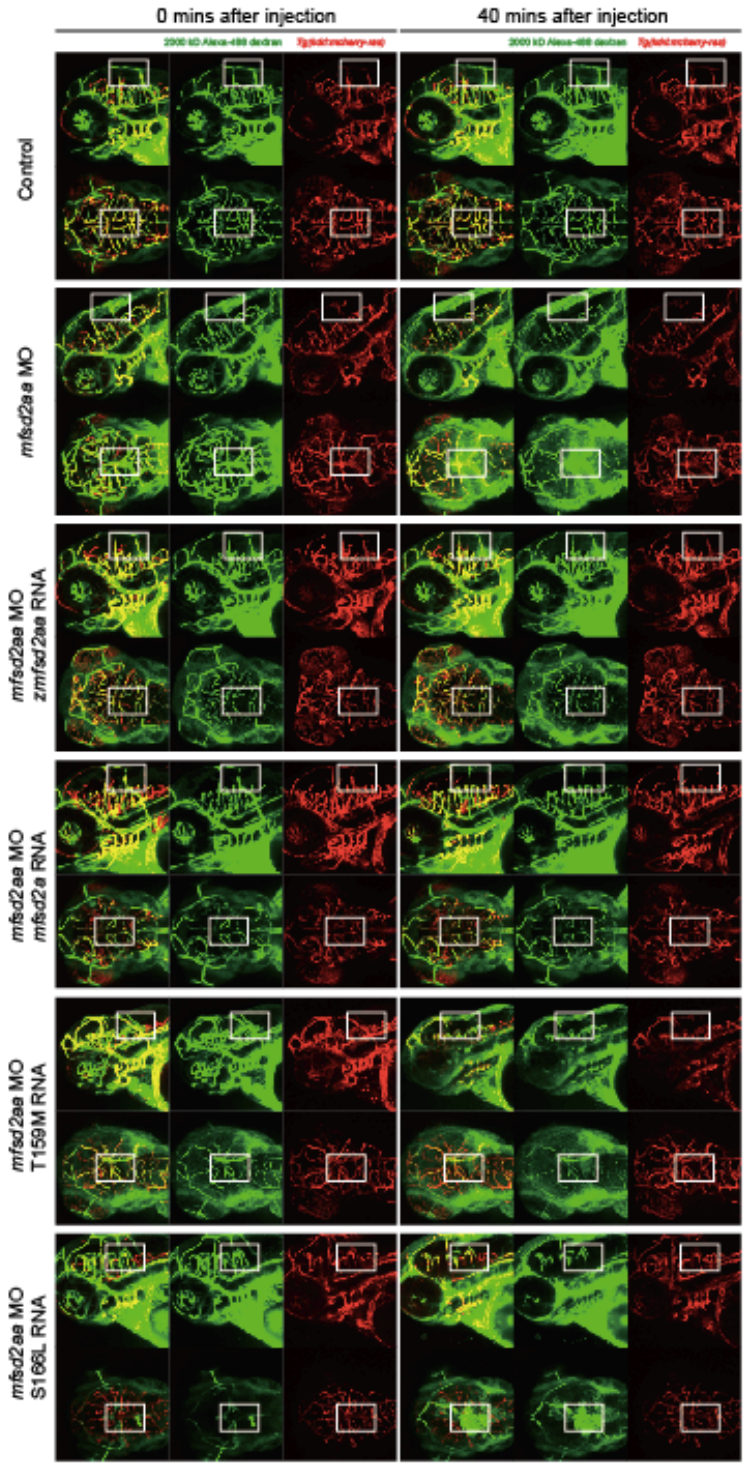

Supplementary Figure 10. 2000 kD dextran injection. Intracardiac injection of 2000-kD dextran into *mfsd2aa* morpholino (MO)-injected and control embryos. *mfsd2aa* MO (1ng) was co-injected with zebrafish wild-type *mfsd2aa* mRNA (50ng), human wild-type *MFSD2A* mRNA (50ng), or mutated p.T159M and p.S166L human *MFSD2A* mRNA (50ng). Colocalization of dextran (green) and cranial blood vessels (red). See **Supplementary videos 7-12**.

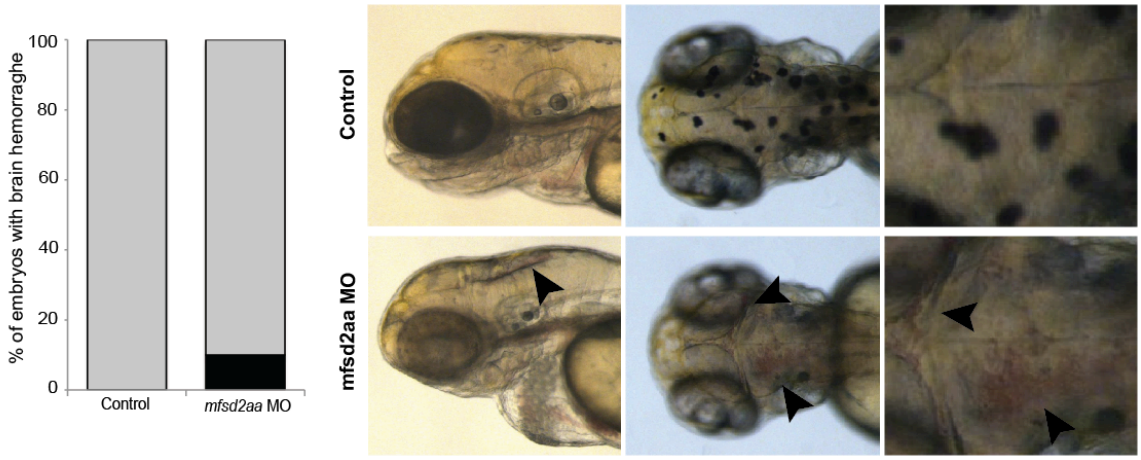

Supplementary Figure 11. *mfsd2aa* morphants exhibit brain hemorrhage. Injection of *mfsd2aa* MOs in zebrafish embryos caused brain hemorrhage (10%) at 3 day post fertilization (dpf). Representative images of control and *mfsd2aa* morphant showing brain hemorrhage (arrowhead).

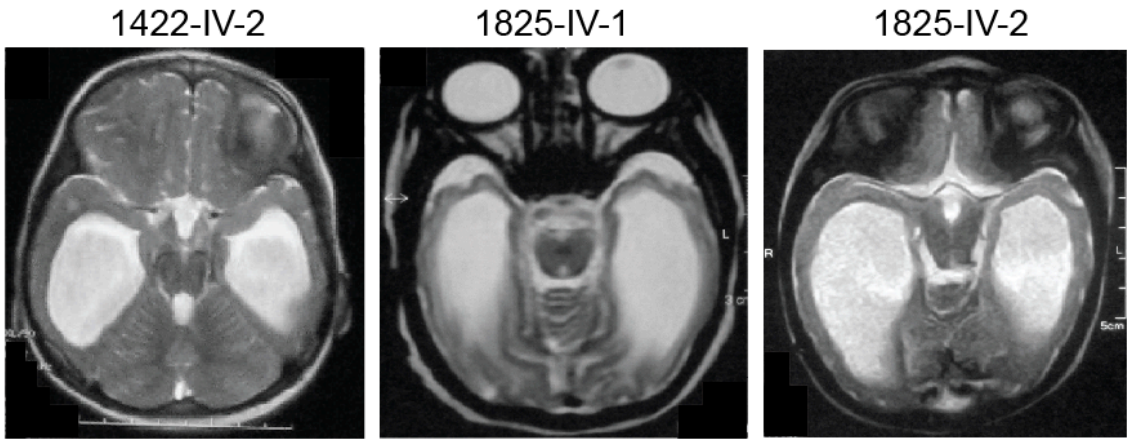

Supplementary Figure 12. Axial MRI T2 images showing absence of evidence of blood derived products determined by this level of resolution in affected children.

Supplementary videos

Supplementary video 1: Intracardiac injection of 10-kD dextran into control embryos. (**a**) side and (**b**) dorsal view 2 minutes after dextran injection. Colocalization of dextran (green) and cranial blood vessels (red). Arrow pointing to brain parenchyma.

Supplementary video 2: Intracardiac injection of 10-kD dextran into *mfsd2aa* morpholino (1ng) (MO)-injected embryos. (**a**) side and (**b**) dorsal view 2 minutes after dextran injection. Colocalization of dextran (green) and cranial blood vessels (red). Arrow pointing to dextran extravasation into the brain parenchyma.

Supplementary video 3: Intracardiac injection of 10-kD dextran into *mfsd2aa* morpholino (MO)-injected embryos. *mfsd2aa* MO (1ng) was co-injected with human wild-type *MFSD2A* mRNA (50ng). (**a**) side and (**b**) dorsal view 2 minutes after dextran injection. Colocalization of dextran (green) and cranial blood vessels (red). Arrow pointing absence of dextran extravasation into the brain parenchyma.

Supplementary video 4: Intracardiac injection of 10-kD dextran into *mfsd2aa* morpholino (MO)-injected embryos. *mfsd2aa* MO (1ng) was co-injected with zebrafish wild-type *mfsd2aa* mRNA (50ng). (**a**) side and (**b**) dorsal view 2 minutes after dextran injection. Colocalization of dextran (green) and cranial blood vessels (red). Arrow pointing absence of dextran extravasation into the brain parenchyma.

Supplementary video 5: Intracardiac injection of 10-kD dextran into *mfsd2aa* morpholino (MO)-injected embryos. *mfsd2aa* MO (1ng) was co-injected with mutated p.S166L human *MFSD2A* mRNA (50ng). (**a**) side and (**b**) dorsal view 2 minutes after dextran injection. Colocalization of dextran (green) and cranial blood vessels (red). Arrow pointing dextran extravasation into the brain parenchyma.

Supplementary video 6: Intracardiac injection of 10-kD dextran into *mfsd2aa* morpholino (MO)-injected embryos. *mfsd2aa* MO (1ng) was co-injected with mutated p.T159M human *MFSD2A* mRNA (50ng). (**a**) side and (**b**) dorsal view 2 minutes after dextran injection. Colocalization of dextran (green) and cranial blood vessels (red). Arrow pointing dextran extravasation into the brain parenchyma.

Supplementary video 7: Intracardiac injection of 2000-kD dextran into control embryos. (**a**) side and (**b**) dorsal view 0 minutes after dextran injection. (**c**) side and (**d**) dorsal view 40 minutes after dextran injection. Colocalization of dextran (green) and cranial blood vessels (red). Arrow pointing to brain parenchyma.

Supplementary video 8: Intracardiac injection of 2000-kD dextran into *mfsd2aa* morpholino (1ng) (MO)-injected embryos. (**a**) side and (**b**) dorsal view 0 minutes after dextran injection. (**c**) side and (**d**) dorsal view 40 minutes after dextran injection. Colocalization of dextran (green) and cranial blood vessels (red). Arrow pointing to dextran extravasation into the brain parenchyma.

Supplementary video 9: Intracardiac injection of 2000-kD dextran into *mfsd2aa* morpholino (MO)-injected embryos. *mfsd2aa* MO (1ng) was co-injected with human wild-type *MFSD2A* mRNA (50ng). (**a**) side and (**b**) dorsal view 0 minutes after dextran injection. (**c**) side and (**d**) dorsal view 40 minutes after dextran injection. Colocalization of dextran (green) and cranial blood vessels (red). Arrow pointing absence of dextran extravasation into the brain parenchyma.

Supplementary video 10: Intracardiac injection of 2000-kD dextran into *mfsd2aa* morpholino (MO)-injected embryos. *mfsd2aa* MO (1ng) was co-injected with zebrafish wild-type *mfsd2aa* mRNA (50ng). (**a**) side and (**b**) dorsal view 0 minutes after dextran injection. (**c**) side and (**d**) dorsal view 40 minutes after dextran injection. Colocalization of dextran (green) and cranial blood vessels (red). Arrow pointing absence of dextran extravasation into the brain parenchyma.

Supplementary video 11: Intracardiac injection of 2000-kD dextran into *mfsd2aa* morpholino (MO)-injected embryos. *mfsd2aa* MO (1ng) was co-injected with mutated p.S166L human *MFSD2A* mRNA (50ng). (**a**) side and (**b**) dorsal view 0 minutes after dextran injection. (**c**) side and (**d**) dorsal view 40 minutes after dextran injection. Colocalization of dextran (green) and cranial blood vessels (red). Arrow pointing dextran extravasation into the brain parenchyma.

Supplementary video 12: Intracardiac injection of 2000-kD dextran into *mfsd2aa* morpholino (MO)-injected embryos. *mfsd2aa* MO (1ng) was co-injected with mutated p.T159M human *MFSD2A* mRNA (50ng). (**a**) side and (**b**) dorsal view 0 minutes after dextran injection. (**c**) side and (**d**) dorsal view 40 minutes after dextran injection. Colocalization of dextran (green) and cranial blood vessels (red). Arrow pointing dextran extravasation into the brain parenchyma.

Supplementary Table 1

Patient ID	1422-IV-2	1825-IV-1	1825-IV-2
Country of origin	Libya	Egypt	Egypt
Gender	F	M	F
Parental consanguinity	+	+	+
Mutation cDNA	c.497C>T	c.476C>T	c.476C>T
Mutation protein	p.S166L	p.T159M	p.T159M
Evaluation			
Weight at birth (kg)	3.8	2	3.4
Length at birth (cm)	n/a	48	47
HC at birth (SD)	n/a	-1.5	-0.6
HC at latest examination (SD)	-3.5	-5.3	-6.2
Age of death (years; months)	5;9	1;2	2
Speech	Non-verbal	Non-verbal	Non-verbal
Gait	Non-ambulatory	Non-ambulatory	Non-ambulatory
Head lag	No independent head support	No independent head support	Minimal head support
External dysmorphisms	Not obvious apart from squint	Bilateral talipes equinovarus	Bilateral talipes equinovarus
Neurological findings			
Hypotonia	+	+	+
Ataxia	-	-	-
Spastic quadriparesis	+	+	+
Hyperreflexia	+	+	+
Intellectual disability	+	+	+
Autistic features	-	+	+
Other	Recurrent pulmonary insufficiency	Recurrent dysphagia	Recurrent dysphagia
Seizures			
Seizures	+ (Clonic)	+ (Tonic)	+ (Tonic)
Seizure onset	2 years	7 days	30 days
MRI findings			
Ventricles	Hugely dilated	Hugely dilated	Hugely dilated
Cerebellum	Atrophy/hypoplasia	Atrophy/hypoplasia	Atrophy/hypoplasia
Cerebral cortex	Effacement, thin corpus callosum	Effacement, thin corpus callosum	Effacement, thin corpus callosum
Brainstem	Hypoplastic	Hypoplastic	Hypoplastic

Supplementary Table 1. Clinical characteristics of affected members of families 1422 and 1825. Abbreviations. HC head circumference, MRI Magnetic resonance imaging, SD Standard deviation, n/a not available.

Supplementary Table 2

Chr	Position	dbSNP	Ref	Mut	Gene	Function GVS	cDNA Position	AA_ Change	Score PhastCons	Vert Phast Cons	SIFT Score	CADD Score	Cons Score GERP	Distance To Splice	Accession
11	2182393	rs384 2740	C	CGCAA	INS	utr-5			0.006	0.006	N/A	7.762	2.730	2	NM_0011 85098.1
1	40431005		C	T	MFSD2A	missense	c.476C>T	p.T159M	1.000	1.000	0	25.5	5.750	2	NM_0327 93.3
2	95815141		GT	G	ZNF514	frameshift	c.1462GT >G	p.H362S fs*57	0.939	0.376	N/A	26.6	2.740	871	NM_0327 88.1
1	32381592		T	TAA	PTP4A2	intron			0.943	0.993	N/A	12.03	5.320	2	NM_0803 91.3

Supplementary Table 2. Genetic variants from family 1825 from exome sequencing. Abbreviations. Chr chromosome, ref reference, mut mutation, cons conservation.

Supplementary Table 3

Chr	position	dbSNP	Ref	Mut	Gene	Function GVS	cDNA Position	AA_ Change	Score Phast Cons	Vert Phast Cons	SIFT Score	CADD Score	Cons Score GERP	Distance To Splice	Accession
2	131704214		T	G	ARGEF4	intron			0.454	0.569	0	8.893	1.590	4	NM_032995.1
5	127710395		A	T	FBN2	missense	c.2021T>A	p.I647N	1.000	1.000	0.05	22.9	4.180	49	NM_001999.3
14	81259453		T	G	CEP128	missense	c.1211A>C	p.N404T	0.962	0.589	1	0.004	-0.935	2	NM_152446.3
5	169661114		A	G	C5ORF58	intron			0.001	0.001	N/A	5.309	-0.058	3	NM_001102609.1
12	86374869		C	T	IMMT	missense	c.1489G>A	p.V497I	1.000	1.000	N/A	7.762	4.820	45	NM_006839.2
14	71570306		C	G	PCNX	missense	c.6015C>G	p.S2005R	1.000	1.000	0	17.1	4.320	81	NM_014982.2
1	40431162		C	T	MFSD2A	missense	c.497C>T	p.S166L	1.000	1.000	0.01	19.73	5.310	20	NM_032793.3
5	115336146		G	A	AQPEP	missense	c.1532G>A	p.R511G	0.749	1.000	0.02	16.94	2.770	17	NM_173800.4

Supplementary Table 3. Genetic variants from family 1422 from exome sequencing.
Abbreviations. Chr chromosome, ref reference, mut mutation, cons conservation.

Supplementary Table 4

Chr	position	dbSNP	Ref	Mut	Gene	Function GVS	cDNA Position	AA_ Change	Score Phast Cons	AF	Cons Score GERP	Distance To Splice	Accession
1	197053373	12677	G	A	ASPM	utr-3			0	0.271	0.292	184	NM_001206846.1
1	197053373	12677	G	A	ASPM	utr-3			0	0.271	0.292	184	NM_018136.4
1	197070815	1412640	T	C	ASPM	coding-synonymous	7566		0.966	0.844	-0.021	1255	NM_018136.4
1	197070901	964201	A	G	ASPM	missense	7480	p.Y2494H	1	0.998	4.83	1341	NM_018136.4
1	197091537	4915337	A	T	ASPM	coding-synonymous	3579		0.137	0.837	0.594	20	NM_001206846.1
1	197091537	4915337	A	T	ASPM	coding-synonymous	3579		0.137	0.837	0.594	20	NM_018136.4
1	197112533	6677082	G	A	ASPM	coding-synonymous	849		0	0.828	-2.39	408	NM_001206846.1
1	197112533	6677082	G	A	ASPM	coding-synonymous	849		0	0.828	-2.39	408	NM_018136.4
8	6296550	2442513	G	T	MCPH1	missense	513	p.R171S	0	0.951	-4.59	68	NM_001172574.1
8	6296550	2442513	G	T	MCPH1	missense	513	p.R171S	0	0.951	-4.59	68	NM_024596.3
8	6302418	2515569	A	G	MCPH1	missense	1175	p.D392G	0	0.995	-11.5	505	NM_001172574.1
8	6302418	2515569	A	G	MCPH1	missense	1031	p.D344G	0	0.995	-11.5	505	NM_001172575.1
8	6302418	2515569	A	G	MCPH1	missense	1175	p.D392G	0	0.995	-11.5	505	NM_024596.3
9	123170733	4837768	C	G	CDK5RAP2	missense	4618	p.V1540L	0.112	0.768	-0.555	14	NM_001011649.1
9	123170733	4837768	C	G	CDK5RAP2	missense	4618	p.V1540L	0.112	0.768	-0.555	14	NM_018249.4
9	123291036	4836822	C	G	CDK5RAP2	missense	865	p.E289Q	0.961	0.894	3.97	15	NM_001011649.1
9	123291036	4836822	C	G	CDK5RAP2	missense	865	p.E289Q	0.961	0.894	3.97	15	NM_018249.4
9	123342259	932975	C	A	CDK5RAP2	utr-5			0.006	0.983	1.88	62	NM_001011649.1
9	123342259	932975	C	A	CDK5RAP2	utr-5			0.006	0.983	1.88	62	NM_018249.4
9	123342275	932974	A	G	CDK5RAP2	utr-5			0	0.979	0.766	78	NM_001011649.1
9	123342275	932974	A	G	CDK5RAP2	utr-5			0	0.979	0.766	78	NM_018249.4
13	25456425	17480581	A	G	CENPJ	utr-3			0.25		0.722	1083	NM_018451.4
13	25457207	9318911	T	C	CENPJ	utr-3			0.001	0.318	1.35	301	NM_018451.4
13	25486911	9511510	G	T	CENPJ	missense	2635	p.S879A	0.045	0.105	-0.951	58	NM_018451.4
13	25486911	9511510	G	T	CENPJ	missense	253	p.P85T	0.001	0.105	2.37	192	NM_018451.4
13	25457004	34780182	ACTT	A	CENPJ	utr-3			0.001	0.010	1.91	501	NM_018451.4

Supplementary Table 4. Genetic variants in genes listed in OMIM database as causative of clinically relevant phenotype from family 1825 exome sequencing. Abbreviations. Chr chromosome, ref reference, mut mutation, cons conservation, AF allele frequency.

Supplementary Table 5

Chr	position	dbSNP	Ref	Mut	Gene	Function GVS	cDNA Position	AA_ Change	Score Phast Cons	Vert Phast Cons	Cons Score GERP	Distance To Splice	Accession
1	197070815	141264 0	T	C	ASPM	coding-synonymous	7566		0.966	0.844 647	0.022	1255	NM_018136.4
1	197070901	964201	A	G	ASPM	missense	7480	p.Y2494H	1	0.998 344	4.78	1341	NM_018136.4
1	197091537	491533 7	A	T	ASPM	coding-synonymous	3579		0.137	0.837 058	-0.088	20	NM_018136.4
1	197112533	667708 2	G	A	ASPM	coding-synonymous	849		0	0.828 78	-1.22	408	NM_018136.4
9	123291036	483682 2	C	G	CDK5RAP2	missense	865	p.E865Q	0.961	0.894 592	3.72	15	NM_001011649.1
9	123291036	483682 2	C	G	CDK5RAP2	missense	865	p.E865Q	0.961	0.894 592	3.72	15	NM_018249.4
9	123342259	932975	C	A	CDK5RAP2	utr-5			0.006	0.983 996	2.36	62	NM_018249.4
9	123342259	932975	C	A	CDK5RAP2	utr-5			0.006	0.983 996	2.36	62	NM_018249.4
9	123342275	932974	A	G	CDK5RAP2	utr-5			0	0.979 305	-1.32	78	NM_018249.4
9	123342275	932974	A	G	CDK5RAP2	utr-5			0	0.979 305	-1.32	78	NM_018249.4
8	6296550	244251 3	G	T	MCPH1	missense	513	p.R171S	0	0.951 849	-3.26	68	NM_024596.3
8	6302154	208391 4	G	T	MCPH1	missense	911	p.R304I	0	0.179 774	-2.18	241	NM_024596.3
8	6302418	251556 9	A	G	MCPH1	missense	1175	p.D392G	0	0.995 171	-11.4	505	NM_024596.3
8	6338306	126744 88	C	A	MCPH1	missense	2045	p.T682N	0	0.205 574	-0.986	72	NM_024596.3

Supplementary Table 5. Genetic variants in genes listed in OMIM database as causative of clinically relevant phenotype from family 1422 exome sequencing. Abbreviations. Chr chromosome, ref reference, mut mutation, cons conservation, AF allele frequency.

Supplementary Table 6

Primers	
hMfsd2aBamHI	5’-ttttttGGATCCcaccatggccaaaggagaaggcgccgag-3’
hMfsd2aXbaI	5’-ttttttTCTAGA ctagaggatgctagccagctctgtggagtc-3’
T159M-F	5’-CTTTGAAACAATGGTCAtGTGTTTCCATGTTCC-3’
T159M-R	5’-GGAACATGGAAACACaTGACCATTGTTTCAAAG-3’
S166L-F	5’-CCATGTTCCCTACTtGGCTCTCACCATGTTC-3’
S166L-R	5’-GAACATGGTGAGAGCCaAGTAGGGAACATGG-3’
z*mfsd2aa*F	5’-atggccagaggcgagggcgccgagcagttctccagc-3’
z*mfsd2aa*R	5’- catccttcattggtctggttacc-3’
z*mfsd2ab*F	5’-atggcaaaaggagagggagcagagc-3’
z*mfsd2ab*R	5’- ttaaaccacattgagctcagtggagt-3’
Morpholino oligonucleotides	
mfsd2aa MO	5’-CCGCTCCTTCTCCTCTTGCCATAAC-3’
mfsd2ab MO	5’-CCTTTTGCCATCTCGCTTTAAAATT-3’

Supplementary Table 6. Primers and morpholino antisense oligonucleotides used in this study.

Supplementary Results

MODELING HUMAN MFSD2A MUTATIONS

We took advantage of the detailed structural information of MelB to provide a molecular basis for the inactivating mutations p.T159M and p.S166L. The overall mechanism of transport of the MFS family has been first inferred from the X-ray structure of glycerol-3-phosphate transporter GlpT from *E. coli,* and confirmed by structures of other MFS family members and more recently including MelB, a close ortholog of MFSD2A[3,8,9]. The model has been described as a "rocker-switch, alternating access" model in which an outward open conformation binds to ligands causing a conformation switch to the inside-open conformation[9]. The energy to drive this conformational change is provided by the binding of cations that flow down their concentration gradients. In the case of MFSD2A, it utilizes sodium to drive the transport of LPC[4]. Indeed, MFSD2A contains a conserved sodium-binding site that has been shown to be essential for sodium-dependent transport of LPC[4].

A molecular explanation for loss of function of p.T159M in the affected children can be inferred from the atomic resolution structure of MelB. Sequence alignment of human MFSD2A and MelB indicated conservation of T159 with T121 in MelB. T121 in MelB faces the sodium-binding site and forms hydrogen bonds with the sodium binding residue D59, which is equivalent to D97 in human MFSD2A (**Fig. 2i**). Both T121 and D59 are required for MelB transport[3]. Threading the human MFSD2A sequence on the MelB model revealed that T159 in human is also in close proximity to the sodium-binding residue D97, which is equivalent to D96 in mouse MFSD2A and essential for function[4]. Similar to p.T159M, p.T121A in MelB is non-functional. Therefore, the p.T159M mutation is predicted to disrupt sodium binding and prevent ligand transport. The p.S166L mutation is also non-functional, and the affected child is a clinical phenocopy of the children having the p.T159M mutation. Interestingly, p.T159M and p.S166L both reside on transmembrane domain 4 (TMD4), which has been proposed to communicate ligand and sodium binding[3,10]. The S166 residue is conserved in all sequenced vertebrates, but not conserved in MelB. Moreover, the S166 residue faces the transport cavity (**Fig. 2i**), suggesting a role in ligand binding. Indeed, S166 corresponding residue in MelB, W128, is critical for melibiose transport[3,10]. Therefore, S166 residue is predicted to play a role in substrate binding by potentially forming a hydrogen bond with the phosphorylcholine headgroup of LPC.